



# The selective oxidation of ethylene glycol and 1,2-propanediol on Au, Pd, and Au–Pd bimetallic catalysts



Michael B. Griffin<sup>a</sup>, Abraham A. Rodriguez<sup>b</sup>, Matthew M. Montemore<sup>c</sup>, John R. Monnier<sup>b</sup>, Christopher T. Williams<sup>b</sup>, J. Will Medlin<sup>a,\*</sup>

<sup>a</sup> University of Colorado Boulder, Department of Chemical and Biological Engineering, UCB 596, Boulder, CO 80309, United States

<sup>b</sup> University of South Carolina, Department of Chemical Engineering, 301 Main Street, Columbia, SC 29208, United States

<sup>c</sup> University of Colorado Boulder, Department of Mechanical Engineering, UCB 427, Boulder, CO 80309, United States

## ARTICLE INFO

### Article history:

Received 1 May 2013

Revised 20 June 2013

Accepted 12 July 2013

### Keywords:

Ethylene glycol  
1,2-Propanediol  
Glycerol  
Palladium  
Gold  
Bimetallic  
Glycolic acid  
Lactic acid  
Rate-limiting step  
Electroless deposition

## ABSTRACT

The oxidation of ethylene glycol (HOCH<sub>2</sub>CH<sub>2</sub>OH) and 1,2-propanediol (HOCH(CH<sub>3</sub>)CH<sub>2</sub>OH) was investigated over Pd/C, Au/C, and a series of bimetallic catalysts prepared by electroless deposition of Au onto Pd/C. In order to explain the enhanced activity of the bimetallic catalysts, the oxidation kinetics of selectively deuterated reagents were investigated. On Au/C and 0.61Au–Pd/C, a primary kinetic isotope effect was observed for d<sub>4</sub>-ethylene glycol (HOCD<sub>2</sub>CD<sub>2</sub>OH), indicating that C–H bond scission is the rate-limiting step. Density functional theory and X-ray photoelectron spectroscopy experiments show a correlation between an increased electron density in Au core orbitals and more favorable thermodynamics for C–H scission as Au is added to Pd. Computational studies suggest that the rate enhancement on the bimetallic surfaces compared to Pd is likely due to a decrease in coverage of strongly bound adsorbates, while the enhancement over Au is likely due to a decrease in the barrier for C–H scission.

© 2013 Elsevier Inc. All rights reserved.

## 1. Introduction

In recent years, there has been an increased interest in the development of ecologically sustainable catalytic processes to convert renewable resources into useful products. Among the most promising of these processes is the aqueous-phase oxidation of alcohols and polyols, which utilizes environmentally friendly reagents and can occur under mild conditions [1–4]. The resulting ketone, ester, aldehyde, and acid products are highly valued intermediates in the fine chemical, pharmaceutical, and agrochemical sectors [5].

Ethylene glycol (HOCH<sub>2</sub>CH<sub>2</sub>OH) and 1,2-propanediol (HOCH(CH<sub>3</sub>)CH<sub>2</sub>OH) are biorenewable molecules that can be oxidized to glycolate (HOCH<sub>2</sub>COO<sup>−</sup>) and lactate (HO(CH<sub>3</sub>)CHCOO<sup>−</sup>) under alkaline conditions. These intermediates are easily hydrogenated to glycolic acid and lactic acid, which can be used in the cosmetic industry and serve as building blocks for the development of degradable polymers [6,7]. Developing a heterogeneous catalytic process for the conversion of ethylene glycol and 1,2-propanediol

to glycolate and lactate would provide a pathway for the sustainable production of these valuable products. Studying ethylene glycol and 1,2-propanediol can also provide useful insights for the oxidation of other complex alcohols. For example, this combination of polyols allows for an exploration of the importance of primary vs. secondary hydroxyl groups in the oxidation mechanism, since ethylene glycol contains two primary hydroxyl groups, whereas 1,2-propanediol contains both a primary and a secondary hydroxyl group.

Supported Pd catalysts are commonly used for oxidation reactions due to their high levels of activity at close to ambient temperatures [2]. However, they are prone to deactivation due to over-oxidation of active sites and poisoning from strongly adsorbed intermediates [4,8,9]. Au nanoparticles have also shown high selectivity and activity for the oxidation of many polyols to monoacids and are more resistant to poisoning, but their performance is variable and strongly dependent on the particle size, shape, choice of support, and reaction conditions [5,10,11]. Interestingly, mixing Pd and Au to form bimetallic catalysts has been shown to enhance oxidation activity, selectivity, and catalyst lifetime [12–16]. In order to explain the increased performance of these bimetallic catalysts, it is important to investigate the

\* Corresponding author. Fax: +1 303 492 4341.

E-mail address: [Will.Medlin@colorado.edu](mailto:Will.Medlin@colorado.edu) (J.W. Medlin).

mechanistic details of each of these systems. On clean Pd surfaces, the classic model for dehydrogenation of alcohols and polyols begins with adsorption through the oxygen atoms, O–H scission, and the formation of an alkoxide intermediate. This is followed by C–H bond scission in the rate-limiting step [4,17,18]. More uncertainty exists on Au surfaces. One explanation, supported by the increased activity under alkaline conditions, suggests that O–H bond scission is the rate-limiting step [19]. However, work done with Au electrodes shows that C–H bond scission is rate-determining [20]. Little is known about the behavior of polyols on Au–Pd bimetallic alloys, and much could be gained through increased insight into the reactivity of these systems.

This work investigates the oxidation of ethylene glycol and 1,2-propanediol under alkaline conditions on Pd/C, Au/C, and Au–Pd/C. Electroless deposition was used to prepare catalysts with various Au/Pd ratios at the catalyst surface, and experiments were carried out using selectively deuterated reagents to determine the rate-limiting step by monitoring for a kinetic isotope effect. The advantage of electroless deposition is that it has been shown to selectively and controllably deposit one metal (in this case Au) onto the surface of another (Pd), creating truly bimetallic catalyst surfaces. A number of experimental and theoretical techniques were utilized to better understand the catalyst composition and the reactions that take place on its surface. The results address fundamental issues associated with the oxidation of polyols on metal surfaces and provide routes toward the development of improved industrial catalysts.

## 2. Materials and methods

### 2.1. Materials

Ethylene glycol and 1,2-propanediol, as well as reagents used for product identification (acetic acid, acetone, formic acid, glycolic acid, glyoxal, glyoxalic acid, hydroxyacetone, lactic acid, methyl glyoxal, oxalic acid, and pyruvic acid) were obtained in high purity from Sigma Aldrich. High-purity deuterated reagents were obtained from Sigma Aldrich (DOCH<sub>2</sub>CH<sub>2</sub>OD, DOCD<sub>2</sub>CD<sub>2</sub>OD) and Fisher Scientific (HOCD<sub>2</sub>CD<sub>2</sub>OH). CP-97 carbon (BASF Catalysis Inc), sodium gold chloride (NaAuCl<sub>4</sub>·3H<sub>2</sub>O, Alfa-Aesar), potassium gold cyanide (KAu(CN)<sub>2</sub>, STREM Chemicals), sodium carbonate pellets (Na<sub>2</sub>CO<sub>3</sub>, J.T. Baker), formaldehyde (CH<sub>2</sub>O, Sigma Aldrich 37% in water), and hydrazine (N<sub>2</sub>H<sub>4</sub>, Sigma Aldrich 37% in water) were used in the preparation of the Au/C and Au–Pd/C catalysts. Sodium hydroxide pellets (NaOH, J.T. Baker) and 18.2 MΩ-cm deionized water (Thermo Scientific Barnstead Nanopure system) were used in the reaction media and for catalyst preparation. Ultra-high-purity oxygen, argon, and hydrogen were obtained from Airgas.

### 2.2. Catalyst preparation

A series of Au–Pd/C bimetallic catalysts was prepared by depositing Au onto a 5 wt% Pd/C catalyst (BASF Catalysis Inc) using an electroless deposition procedure described previously [21]. Potassium gold cyanide was used as the metal salt and hydrazine was used as the reducing agent. Hydrazine is toxic and unstable in its anhydrous form and should be handled in solution if possible. For deposition baths in which the Au concentration was less than 44 ppm, a metal salt-to-reducing agent molar ratio of 1:10 was used. Baths with Au concentrations over 44 ppm were subject to higher decomposition rates of the reducing agent, so a molar ratio of 1:20 was used. The electroless bath volume was held at 200 mL and 0.500 g of 5 wt% Pd/C was used for all catalyst compositions. The bath temperature was held at 313 K and concentrated sodium hydroxide was used to maintain pH 12 for the duration of the

preparation. The bath was stirred for 4 h to ensure complete deposition. The catalysts were then washed with 1 L of deionized water, filtered, and dried at room temperature overnight.

A 1 wt% Au/C catalyst was made using the deposition–precipitation procedure described by Prati et al. [10]. Saturated sodium carbonate was added to a mixture of 0.050 g sodium gold chloride and 10 mL deionized water until a fixed pH of 10 was reached. The mixture was then added to a stirred slurry of 2.55 g of carbon and 25 mL of deionized water. After being stirred at room temperature for 1 h, the slurry was heated to 343 K and 3 mL of formaldehyde was added drop wise over 3 min to ensure complete reduction of Au. This solution was stirred for 1 h before being filtered and dried. Since the Au/C catalysts were prepared using a different technique than the Pd/C and Au–Pd/C catalysts, factors beyond the type of metal may contribute to differences in reactivity.

### 2.3. Catalyst characterization

The concentration of accessible surface Pd sites was determined by chemisorption using hydrogen titration of oxygen pre-covered Pd. For this technique, the catalysts were heated to 473 K at a rate of 10 K/min under a 10% H<sub>2</sub>/90% Ar mixture. The temperature was held at 473 K for 1 h, and then, the catalysts were purged with argon for 30 min before being cooled in argon to 313 K. Next, the catalyst surface was saturated with oxygen by exposing it to 10% O<sub>2</sub>/90% Ar for 30 min. It was then purged with argon for 10 min before being exposed to pulse doses of 0.52 cm<sup>3</sup> of 10% H<sub>2</sub>/90% Ar until all of the surface oxygen was converted to water. Hydrogen consumption was monitored using a high-sensitivity thermal conductivity detector downstream from the sample cell. This technique provides a good indication of the number of active sites exposed on the Pd/C catalyst. Also, since only Pd can dissociate oxygen at 313 K, the Au coverage on the bimetallic catalysts can be estimated by calculating the ratio of active sites before and after electroless deposition [22]. While oxygen can potentially “spillover” [23] and bind to surface Au atoms, the low adsorption energy of O on Au surfaces (Section 3.5) suggests that room-temperature coverage should be low. Moreover, assuming negligible O coverage on Au is consistent with the results presented below, where low amounts of deposited Au are found to eliminate approximately one adsorption site per Au atom deposited [21,24,25].

The Au/C catalysts were characterized using X-ray diffraction (XRD). These experiments were performed on a Rigaku Miniflex II desktop X-ray diffractometer equipped with a D/tex Ultra detector with a Cu K-alpha radiation source; scans were performed from 10 degrees to 80 degrees, with a step size of 0.020 degrees and a scan speed of 0.500 degrees/min. The PDXL software package from Rigaku was used to analyze data and calculate average particle sizes.

X-ray photoelectron spectroscopy (XPS) experiments were carried out on the bimetallic Au–Pd/C catalysts using a Kratos Axid Ultra DLD XPS system equipped with a hemispherical energy analyzer. The monochromatic Al K $\alpha$  X-ray source was operated at 15 keV and 120 W, incident at 45 degrees to the surface normal. The pass energy was fixed at 40 eV for detailed scans of the Au 4f region. Scans were performed on catalysts as synthesized and after in situ reduction under hydrogen at 473 K for 1 h. For comparison, AuCl<sub>3</sub><sup>-</sup> and Au(CN)<sub>2</sub><sup>-</sup> were used to prepare 1 wt% Au/C catalysts as references for the Au(III) and Au(I) states respectively and were analyzed as prepared. Transmission electron microscopy (TEM) was conducted using a JEOL 2100F high-resolution instrument.

### 2.4. Reaction studies

The aqueous-phase oxidation of ethylene glycol and 1,2-propanediol was performed in a 100 mL EZE-Seal™ batch reactor

(Autoclave Engineers). At the beginning of each run, the reactor was filled with 70 mL of deionized water, 3.2 g of sodium hydroxide, and a specified amount of catalyst. The vessel was sealed and heated to 333 K. Once the desired temperature was reached, 10 mL of reagent was injected using a syringe, and the reactor was pressurized with 145 psig of oxygen. The reaction mixture was stirred vigorously at 1200 rpm. Liquid samples were withdrawn using a custom dip tube and analyzed using a Shimadzu-10AVP high-pressure liquid chromatography system equipped with both ultraviolet (SPD-10AVP) and refractive index (RID-10A) detectors. The compounds were separated in an ion exclusion column (Alltech OA-1000 Organic Acids) at 353 K, with 0.005 M sulfuric acid solution flowing at 0.600 mL/min as the mobile phase. The retention times and calibration curves of products were determined by analyzing samples of known concentration.

The turnover frequencies for each of the catalysts were calculated based on the moles of reagent consumed during the initial reaction phase, in which the concentration decreased in a nearly linear fashion. This was scaled by number of active sites, which was determined by chemisorption for the monometallic Pd catalysts. The number of accessible metal atoms on the bimetallic catalysts is considered to be equal to that of the monometallic Pd catalysts upon which they are based. This assertion is based on the assumption of catalytic deposition, which is supported by the XPS results (Section 3.1) and has been shown to dominate at lower weight loadings when group IB metals are deposited on Pd catalysts using electroless deposition [21]. However, it is possible that large clusters of Au are formed due to autocatalytic deposition at high Au loadings [21]. The average particle size and dispersion of the Au/C catalysts were determined using XRD. These values were then used to estimate the number of active sites and calculate turnover frequencies.

Confidence intervals ( $\alpha = 0.025$ ) on the fits used to calculate the turnover frequencies and rate constants were established by a simple regression analysis using the method of least squares. Logarithmic transformations used to calculate the rate constants resulted in a large number of data points in the linear range for these fits. Similar transformations were not carried out for the turnover frequency data since the initial concentrations in these experiments was higher, leading to a larger range of concentration values and possible violations of homoscedasticity. Instead, the turnover frequency was calculated based on the moles consumed during the initial reaction phase, in which the concentration decreased in a nearly linear fashion. This range contains fewer data points, resulting in wider confidence intervals on these calculations. While this method provides a good indication of how well the slope of the fit matches the actual data and can account for sampling variability within experiments, it does not directly measure the reproducibility of the results.

### 2.5. Density functional theory calculations

Plane-wave density functional theory (DFT) calculations were performed with the Vienna ab initio Simulation Package (VASP) and the PW91 exchange–correlation functional with a basis set cut-off of 396 eV [26–28] and the projector augmented wave method [29,30]. For core-level shift calculations, a  $13 \times 13 \times 1$  k-point mesh was used, while a  $7 \times 7 \times 1$  k-point mesh was used for adsorption energy calculations. A  $2 \times 2$  surface cell was used with four layers of substrate. Core-level shifts were calculated using only initial state effects, i.e., shifts were computed as differences between core-level energies computed by DFT, and core relaxation effects upon electron excitation were ignored. This has been previously shown to be a good approximation for calculating trends in core-level shifts in transition metals, particularly for (111) surfaces, though it is less accurate than including final-state effects [24,31,32]. For adsorption calculations, dispersion interac-

tions were included using the DFT-D2 method [33]. The values of  $C_6$  and the van der Waals radius for Au,  $40.62 \text{ J nm}^6 \text{ mol}^{-1}$  and 0.1772 nm, were taken from a previous publication [34]. Dispersion interactions were found to have a negligible effect on adsorbate geometries except in the cases of formaldehyde on Au(111) and methanol on all surfaces. Visualizations were created using QuteMole [35].

## 3. Results

### 3.1. Catalyst preparation and characterization

From chemisorption, a dispersion of 24% and average particle size of 4.4 nm were measured for the Pd/C catalyst. TEM measurements shown in Fig. 1(a) indicate Pd particle sizes ranging from approximately 1.5 nm–5 nm, with an average around 3 nm. Since Au cannot reliably dissociate oxygen, XRD was used instead of chemisorption to characterize the Au/C catalysts. Two Au catalysts were used with average particle sizes of 13 nm and 18 nm and 8.5% and 6.4% dispersion, respectively.

A series of bimetallic Au–Pd/C catalysts were prepared to obtain increasing fractional coverage of Au on Pd using electroless

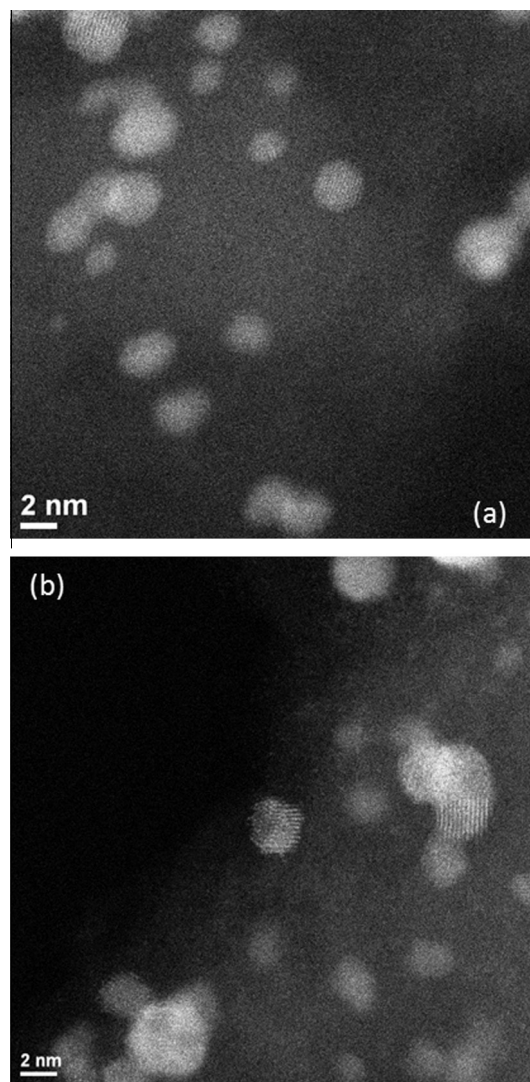


Fig. 1. TEM images of the (a) 5 wt% Pd/Al<sub>2</sub>O<sub>3</sub> catalyst and (b) the same catalyst covered with 0.60 ML Au (0.60Au-Pd/Al<sub>2</sub>O<sub>3</sub>).

**Table 1**  
Theoretical and actual Au coverage of Au–Pd/C catalysts prepared by electroless deposition.

Theoretical coverage	Real coverage	Au wt%
0.50	0.36	1.14
0.65	0.45	1.48
0.71	0.60	1.61

deposition [21]. Table 1 shows the theoretical Au coverage assuming a one-to-one stoichiometry with underlying Pd atoms, along with the actual Au coverages determined by chemisorption for various bath compositions. As expected, autocatalytic deposition of Au occurs at high coverage, which explains the deviation from theoretical values. These results are consistent with a previous study of Au–Pd catalysts on SiO<sub>2</sub> prepared by electroless deposition, where higher Au loadings than those corresponding to full mono-dispersed coverage resulted in only partial Au coverages [21,25]. TEM images of a 0.60Au–Pd catalyst (Fig. 1(b)) indicate particle sizes ranging from 1.8 to 6.5 nm, with an average of just over 3 nm.

The bimetallic catalysts were also analyzed by XPS in order to investigate their electronic structure (Fig. 2). The carbon 1s peak was used as an internal standard to confirm the position of the peaks. Since the carbon support is conductive, the peak positions can be compared without any further corrections. For the bimetallic compositions analyzed, a shift to lower binding energies was observed for the Au 4f<sub>5/2</sub> and Au 4f<sub>7/2</sub> peaks in comparison with a 1 wt% Au/C catalyst. Furthermore, this shift increased as the Au coverage was decreased, consistent with larger electronic effects on more dispersed Au atoms. These shifts to lower binding energy are also consistent with previous studies of Au–Pd bimetallic nanoparticles [25,36–39]. These experimental core-level shifts are in excellent agreement with DFT calculations for a bimetallic (111) surface alloy up to a high coverage of Au on Pd (Fig. 3). At this high coverage, Au deposited autocatalytically onto other Au atoms is expected to contribute to the signal, perhaps accounting for the greater deviation. The core-level shifts for Au adsorbed in the fcc hollow site of Pd(111) at 0.25 ML and 0.5 ML coverage were also investigated; these showed the same trend but at a much larger magnitude (0.85 eV for 0.25 ML and 0.60 eV for 0.50 ML). This suggests that the surface alloy is a better model for the bimetallic

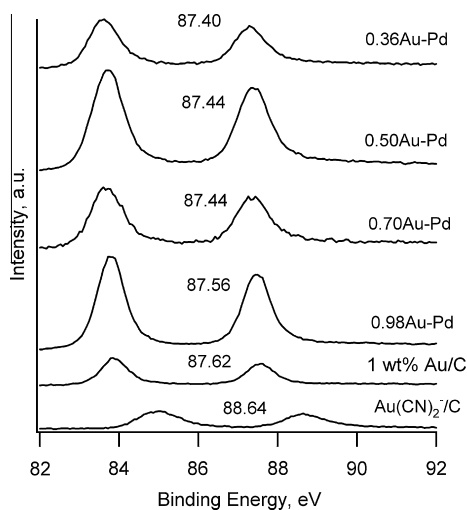


**Fig. 2.** Au 4f<sub>5/2</sub> and Au 4f<sub>7/2</sub> peaks from XPS experiments carried out on various Au–Pd/C bimetallic catalysts. Peak locations were confirmed by comparison with the carbon 1s peak (data not shown).

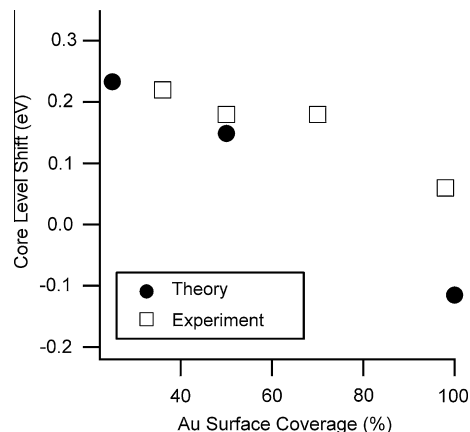


**Fig. 3.** The magnitude of the Au core-level shifts for bimetallic catalysts with varying Au composition as determined by XPS and DFT.

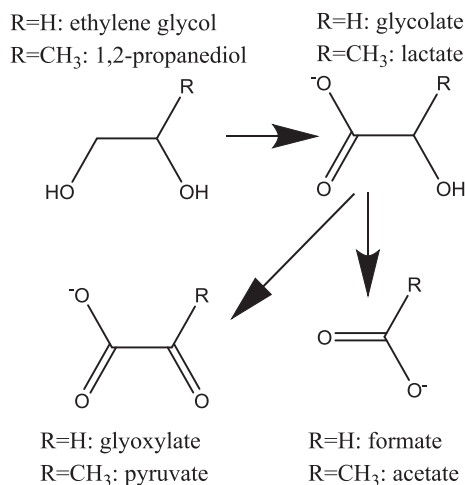
catalysts and that geometric effects do not play a large role in the experimentally observed shifts.

Previous reports have attributed the core-level shift to electron transfer from Pd to Au [21]. However, the DFT calculations indicate that there is little change in the filling of the d-bands, which is consistent with previous work on late transition metal alloys [40,41]. This indicates that charge transfer may not be the correct picture for core-level shifts. Instead, changes in the embedding density and potential [40] or, in the same vein, the atomic coupling [41] are more likely to be the causes of the shifts. (The same mechanisms are likely the cause of d-band center shifts in late transition metal alloys [40].) Essentially, since the Au atoms are larger than the Pd atoms, embedding Au atoms in the Pd lattice results in increased overlap and hence more electron density near the Au cores. This causes the Au core electrons to be less strongly bound in the alloy than in pure Au.

### 3.2. Ethylene glycol oxidation

The oxidation of ethylene glycol was carried out in the aqueous phase on 5 wt% Pd/C, 1 wt% Au/C, and various loadings of Au–Pd/C catalysts prepared by electroless deposition of Au onto Pd/C. The initial reaction mixture was comprised of 0.1 M ethylene glycol and 1.0 M sodium hydroxide. The temperature was held at 333 K, and the reaction vessel was pressurized to 145 psig with oxygen while being stirred at 1200 rpm. The experiments on Pd/C and Au–Pd/C were carried out on 60 mg of catalyst, while 150 mg of Au/C was used due to the lower metal loading. Product analysis indicated that oxidation of one of the ethylene glycol hydroxyl groups to glycolate (see Scheme 1) was the only observed pathway on any of the catalysts.

Fig. 4 displays the effect of reaction time on ethylene glycol conversion for Pd/C, Au/C, and 0.45Au–Pd/C catalysts. On the bimetallic catalyst, nearly 90% conversion was achieved in 3 h. Low activity was observed on Pd/C and Au/C. The initial turnover frequency for each experiment was calculated in order to standardize the results with respect to number of available active sites (Table 2). The Pd/C catalyst showed low activity toward ethylene glycol oxidation, with an initial turnover frequency of approximately 45 h<sup>-1</sup>. Oxidation on Au/C was also slow, with a turnover frequency of 42 h<sup>-1</sup>. However, each of the bimetallic catalysts showed a significant increase in activity, with turnover frequencies of 390 h<sup>-1</sup> for 0.35Au–Pd/C, 590 h<sup>-1</sup> for 0.36Au–Pd/C, 530 h<sup>-1</sup> for 0.45Au–Pd/C, 530 h<sup>-1</sup> for 0.61Au–Pd/C, and 600 h<sup>-1</sup> for 0.92Au–Pd/C. As shown in Table 1 and Fig. 3, the autocatalytic deposition of Au is likely at high loadings. For this reason, it is possible that the turnover



**Scheme 1.** Oxidation pathways observed in the present study for ethylene glycol and propanediol oxidation. For simplicity, oxidizing species and C<sub>1</sub> products are not shown.

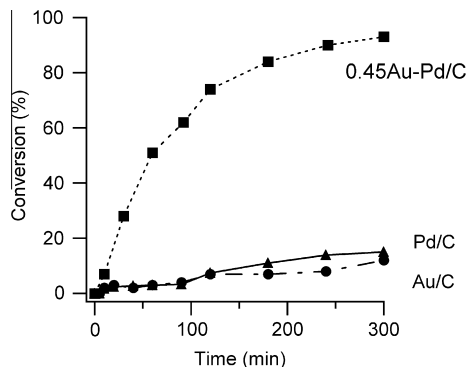


**Fig. 4.** Ethylene glycol conversion vs. time for 60 mg of 5 wt% Pd/C, 150 mg of 1 wt% Au/C, and 60 mg of 0.45Au–Pd/C.

**Table 2**  
The selective oxidation of ethylene glycol to glycolate.

Catalyst	TOF (1/h)	Selectivity (%)	Mole balance (%)
5% Pd/C	45 (±82)	100	93
0.35Au–Pd/C	390 (±79)	100	100
0.36Au–Pd/C	570 (±110)	100	97
0.45Au–Pd/C	530 (±105)	100	97
0.61Au–Pd/C	530 (±106)	100	96
0.92Au–Pd/C	600 (±160)	100	99
1% Au/C	42 (±36)	100	100

Selectivity/mole balance at ~10% conversion.  
Confidence interval at  $\alpha = 0.025$ .

frequency of the 0.92Au–Pd/C catalyst is inflated due to presence of extra active sites that are not accounted for in these calculations. Table 2 also shows the selectivity and mole balance for each experiment. Selectivity was 100% to glycolate at all measured conversions and the mole balance was >90% for each of the catalysts. The results on the monometallic catalysts are consistent with a previous study by Bianchi and coworkers in which ethylene glycol oxidation on 5 wt% Pd/C and 1 wt% Au/C also resulted in the selective production of glycolate [10].

### 3.3. 1,2-Propanediol oxidation

The oxidation of 1,2-propanediol was investigated on 5 wt% Pd/C, 1 wt% Au/C, and various loadings of Au–Pd/C bimetallic catalysts

prepared by electroless deposition. In all cases, the reaction conditions were identical to the ethylene glycol experiments. In addition to the major product lactate, small amounts of pyruvate and acetate (Scheme 1) were detected in the product in some cases. The effect of reaction time on 1,2-propanediol conversion for Pd/C, Au/C, and 0.45Au–Pd/C catalysts can be seen in Fig. 5a. The enhanced activity of the bimetallic catalyst is consistent with the results obtained for ethylene glycol oxidation. Fig. 5b shows the catalyst selectivity to lactate as a function of time. On Pd/C and 0.45Au–Pd/C, the selectivity remained relatively constant at >97%. On Au/C, the selectivity was initially near 100% but started to drop at ~10% conversion. The decrease in selectivity was due to an increased production of acetate. The initial turnover frequencies are shown in Table 3. The turnover frequency on Pd/C was only 25 h<sup>-1</sup>. The Au/C catalyst was more active than the Pd catalyst, with a turnover frequency of 300 h<sup>-1</sup>, but the bimetallic catalysts showed the highest turnover frequencies at 550 h<sup>-1</sup> for 0.35Au–Pd/C, 670 h<sup>-1</sup> for 0.36Au–Pd/C, 760 h<sup>-1</sup> for 0.45Au–Pd/C, 680 h<sup>-1</sup> for 0.61Au–Pd/C, and 940 h<sup>-1</sup> for 0.92Au–Pd/C. As shown in Table 1 and Fig. 3, the autocatalytic deposition of Au is likely at high loadings. For this reason, it is possible that the turnover frequency of the 0.92Au–Pd/C catalyst is inflated due to presence of extra active sites that are not accounted for in these calculations. This is further supported by the larger increase in activity for 1,2-propanediol relative to ethylene glycol on this catalyst, since monometallic Au is more active for the oxidation of 1,2-propanediol. The large uncertainty associated with the measurement of 0.92Au–Pd/C is due to the limited number of data points within the linear range used to determine the turnover frequency.

Table 3 also shows the selectivity and mass balance at ~10% conversion. Lactate (HOCH(CH<sub>3</sub>)COO<sup>-</sup>) was the primary product for each of the catalysts tested. Pyruvate (CO(CH<sub>3</sub>)CH<sub>2</sub>O<sup>-</sup>) and acetate (CH<sub>3</sub>COO<sup>-</sup>) were also produced in small amounts. The mole balances for the monometallic catalysts were each above 90%. The mole balances for the bimetallic catalysts were between 80% and 90% at low conversion, but improved to above 90% as conversion increased. These results are in agreement with previous studies of 1,2-propanediol oxidation under various conditions on similar catalysts, which also showed the selective production of lactate and an increased activity associated with Au–Pd bimetallic catalysts [10,42].

To test for loss of catalyst activity over the reaction period, a smaller amount (0.20 g) of the 0.45Au–Pd catalyst was also evaluated under the same experimental conditions. This decreased the PDO conversion to approximately 70% over 5 h and allowed for an evaluation of whether extended exposure to the reactants led to appreciable deactivation. Variation in the measured turnover frequency was within experimental error, and the catalyst exhibited negligible deviations from a first-order decay curve up to 5 h (maximum deviation of 2% with apparently random scatter). Thus, though deactivation over long timescales cannot be ruled out, deactivation appears minimal over the timescale of the experiments.

### 3.4. Ethylene glycol isotope experiments

Oxidation experiments were carried out with selectively deuterated ethylene glycol in order to probe for a kinetic isotope effect. In all cases, the initial concentration of ethylene glycol was 0.01 M, the initial concentration of sodium hydroxide was 1.0 M, the temperature was held at 333 K, and the vessel was pressurized with oxygen to 145 psig while being stirred at 1200 rpm. Substituting deuterium for hydrogen allows for insight into the oxidation kinetics, since it will slow the reaction if the isotopic replacement occurs in a bond that is broken during the rate-limiting step [43]. For this reason, a comparison between the oxidation rates of d<sub>0</sub>-ethylene

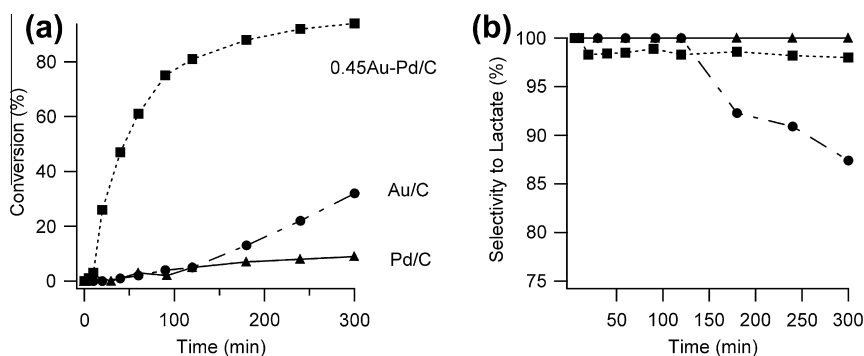


Fig. 5. 1,2-Propanediol conversion vs. time (a) and selectivity to lactate vs. time (b) for 60 mg of 5 wt% Pd/C, 150 mg of 1 wt% Au/C, and 60 mg of 0.45Au-Pd/C.

**Table 3**  
The selective oxidation of 1,2-propanediol to lactate.

Catalyst	TOF (1/h)	Selectivity (%)	Mole balance (%)
5% Pd/C	25 ( $\pm 82$ )	100	97
0.35Au-Pd/C	550 ( $\pm 100$ )	99	90
0.36Au-Pd/C	670 ( $\pm 130$ )	100	80
0.45Au-Pd/C	760 ( $\pm 190$ )	99	90
0.61Au-Pd/C	680 ( $\pm 300$ )	99	85
0.92Au-Pd/C	940 ( $\pm 660$ )	94	79
1% Au/C	300 ( $\pm 77$ )	87	94

Selectivity/mole balance at  $\sim 10\%$  conversion.

Confidence interval at  $\alpha = 0.025$ .

glycol (HOCH<sub>2</sub>CH<sub>2</sub>OH), d<sub>2</sub>-ethylene glycol (DOCH<sub>2</sub>CH<sub>2</sub>OD), d<sub>4</sub>-ethylene glycol (HOCD<sub>2</sub>CD<sub>2</sub>OH), and d<sub>6</sub>-ethylene glycol (DOCD<sub>2</sub>CD<sub>2</sub>OD) provides a simple method for determination of whether C–H or O–H scission is the rate-limiting step. The reaction order with respect to ethylene glycol was determined by comparison with the integrated rate laws. The best linear fits were obtained when plotting the natural log of concentration versus time, which indicates first-order kinetics and is consistent with the oxidation of various alcohols, aldehydes, and ketones on Pt and Pd [44]. The apparent rate constants for the oxidation of selectively deuterated ethylene glycol on 0.61Au-Pd/C and Au/C are shown in Table 4.

On the bimetallic catalyst, there is no evidence of a primary kinetic isotope effect during the oxidation of d<sub>2</sub>-ethylene glycol, suggesting that the overall kinetics are unaffected by the incorporation of deuterium into the hydroxyl groups. However, it is possible that under these reaction conditions, the exchange of hydrogen and deuterium can occur between water and hydroxyl groups. Early studies suggested that this process takes about 18 h to reach equilibrium, making it unlikely to influence these experiments [45]. However, other work has shown that the exchange occurs quickly [46]. For this reason, the possibility of hydrogen-deuterium exchange cannot be eliminated, and it remains possible that the O–H bond activation energy may affect the overall kinetics. However, the results show evidence of a primary kinetic isotope effect for d<sub>4</sub>-ethylene glycol. In these experiments, a  $k_H/k_D$  of  $\sim 5$  was detected for d<sub>4</sub>-ethylene glycol. This value agrees

**Table 4**  
Rate constants (1/h) for deuterated ethylene glycol oxidation.

Reagent	0.61Au-Pd/C <sup>a</sup>	$k_H/k_D$ (Confidence interval)	1% Au/C <sup>b</sup>	$k_H/k_D$ (Confidence interval)
d <sub>0</sub> -EG (HOCH <sub>2</sub> CH <sub>2</sub> OH)	0.35 ( $\pm 0.02$ )	–	0.019 ( $\pm 0.003$ )	–
d <sub>2</sub> -EG (DOCH <sub>2</sub> CH <sub>2</sub> OD)	0.28 ( $\pm 0.02$ )	1.3 (1.1–1.4)	0.011 ( $\pm 0.003$ )	1.7 (1.1–2.7)
d <sub>4</sub> -EG (HOCD <sub>2</sub> CD <sub>2</sub> OH)	0.07 ( $\pm 0.02$ )	4.7 (3.7–6.3)	0.0015 ( $\pm 0.003$ )	13 (>3.6)
d <sub>6</sub> -EG (DOCD <sub>2</sub> CD <sub>2</sub> OD)	0.04 ( $\pm 0.02$ )	8.8 (5.6–18)	0.0032 ( $\pm 0.002$ )	6.0 (3.0–21)

<sup>a</sup> 0.01 M EG, 1.0 M NaOH, 1 MPa O<sub>2</sub>, 30 mg catalyst.

<sup>b</sup> 0.01 M EG, 1.0 M NaOH, 1 MPa O<sub>2</sub>, 150 mg catalyst All confidence intervals based on  $\alpha = 0.025$ .

(within error) with theoretical calculations of a primary kinetic isotope effect for hydrogen–deuterium exchange and is consistent with previous investigations that show a  $k_H/k_D$  of  $\sim 4$  for liquid phase oxidation of d<sub>2</sub>-ethanol (CH<sub>3</sub>CD<sub>2</sub>OH) with bromine under similar reaction conditions [43,47]. These results suggest that C–H bond scission is the rate-limiting step on 0.61Au-Pd/C.

Rate constants on Au/C are all smaller than on the bimetallic catalysts, but the results show similar trends. The reaction rate of d<sub>4</sub>-ethylene glycol was suppressed by a factor of  $\sim 13$ . These results suggest that C–H bond scission is also rate-limiting on Au/C and agree with previous computational studies of the oxidation of ethanol in which C–H bond scission was shown to have the highest activation barrier on Au under basic conditions [48].

### 3.5. Density functional theory calculations

Since the experimental results indicate that C–H scission is the rate-determining step, C–H scission was studied using DFT, using methoxy as a simple proxy for the alkoxides. The adsorption energy of the most stable configurations of methanol, methoxy, formaldehyde, water, hydroxyl, H, and O were found on Pd(111), Au(111), and surface alloys with 0.25 ML and 0.5 ML of Au in Pd(111). The adsorption energies relative to combinations of the stable gas-phase species H<sub>2</sub>, O<sub>2</sub>, H<sub>2</sub>O, CH<sub>2</sub>O, and CH<sub>3</sub>OH are in Table 5, and selected images are in Fig. 6. The site preference is generally the same across the different surfaces,

**Table 5**  
Adsorption energies in eV of various adsorbates, with the site preference in parentheses (f = fcc, b = bridge, t = top).

Surface	H	O	OH	H <sub>2</sub> O	CH <sub>2</sub> O	CH <sub>3</sub> O	CH <sub>3</sub> OH
Pd(111)	–0.67 (f)	–1.59 (f)	0.36 (b)	–0.57 (t)	–1.10 (f)	0.12 (f)	–0.73 (t)
0.25Au-Pd(111)	–0.70 (f)	–1.47 (f)	0.44 (b)	–0.58 (t)	–1.04 (f)	0.18 (f)	–0.75 (t)
0.50Au-Pd(111)	–0.50 (f)	–0.81 (f)	0.54 (b)	–0.57 (t)	–0.91 (b)	0.37 (b)	–0.77 (t)
Au(111)	–0.12 (f)	–0.21 (f)	1.21 (f)	–0.40 (t)	–0.42 (t)	0.89 (f)	–0.58 (t)

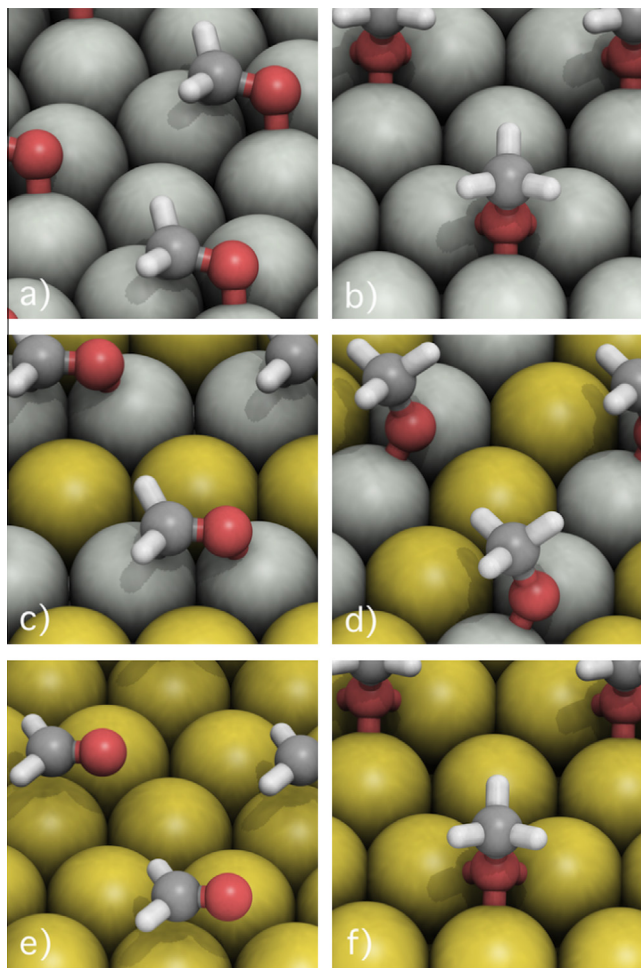


**Fig. 6.** Adsorption geometries of formaldehyde and methoxy on (a and b) Pd(111), (c and d) 0.5Au–Pd(111), and (e and f) Au(111).

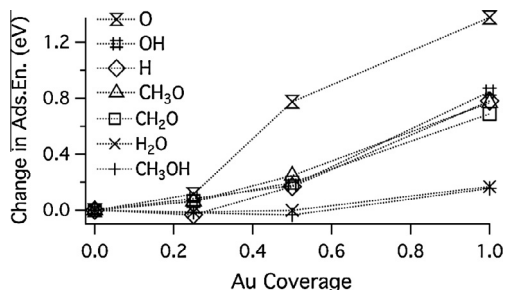


**Fig. 7.** The adsorption energy relative to Pd(111) as a function of the Au coverage, where a coverage of 1 indicates Au(111).

with the notable variation that methoxy and formaldehyde prefer the bridge site on the 0.5 ML Au–Pd(111) surface, likely because all hollow sites have at least one Au atom. In general, the adsorption energy increases as the Au coverage increases, indicating that Au destabilizes adsorbates (Fig. 7). Most of the adsorbates experience very similar destabilizations; the exceptions are water and methanol, which are destabilized much less, and O, which is destabilized much more.

As noted in previous work, there are several possible mechanisms for dehydrogenation of methoxy to formaldehyde, including transfer of the H atom to the surface, to another methoxy species, to an adsorbed O atom, or to an adsorbed hydroxyl [49]. The reaction energies of all of these pathways are given in Table 6. Transfer

**Table 6**  
Reaction energies in eV of CH<sub>3</sub>O dehydrogenation for H transfer to various species.

Surface	To surface	To OH	To O	To CH <sub>3</sub> O
Pd(111)	−0.53	−0.71	−0.49	−0.79
0.25Au–Pd(111)	−0.56	−0.79	−0.52	−0.88
0.50Au–Pd(111)	−0.41	−1.04	−1.14	−1.02
Au(111)	0.18	−1.40	−1.10	−1.55

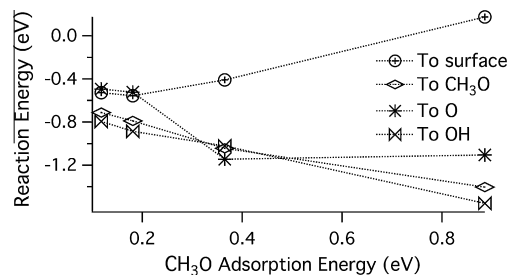


**Fig. 8.** The reaction energy of H transfer from methoxy to various species as a function of the methoxy adsorption energy.

of H to O, OH, or methoxy becomes more favorable as the Au coverage increases, while transfer of H to the surface becomes less favorable. These trends correlate with the methoxy adsorption energy, as shown in Fig. 8. These trends may explain previous findings that H is transferred to the surface on Pt(111) but transferred to OH on Au(111) for ethoxy dehydrogenation [48].

To further understand C–H scission, barriers for the reaction step were calculated on Pd(111), 0.5Au–Pd(111), and Au(111). Previous work has shown that on Au(111), surface OH facilitates C–H bond scission in ethoxy [48]. Other work has shown that transfer of the H to OH and directly to the surface have similar barriers for methoxy dehydrogenation on Au(111) [49]. Therefore, on Au(111) only the transfer of H to OH was considered. For Pd(111) and 0.5Au–Pd(111), transfer of H to both OH and the surface were studied in order to find the more favorable pathway.

Potential energy diagrams of all of these processes are shown in Fig. 9. On Pd(111), methoxy can undergo two C–H scission pathways. In the first (black line in Fig. 9a), dissociation occurs with the methoxy O atom bound in a Pd–Pd bridge site; in the second, methoxy undergoes a second diffusion step so that the dissociation precursor is bound atop a single Pd atom. The transition state for methoxy dissociation in the bridge site has a slightly lower energy (by about 0.1 eV). The C–H dissociation barrier of ~0.5 eV is consistent with that observed in surface science investigations. The barrier on Pd(111) is only subtly affected when surface OH is present. C–H scission occurs from a precursor in which OH is adsorbed in the top site and methoxy in the bridge site. On the Au(111) surface, dissociation occurs from a precursor in which methoxy is in a top position and OH in a bridge, as observed previously [49]. Surface OH stabilized both the precursor and transition states for methoxy decomposition.

On the bimetallic PdAu(111) surface, the much weaker binding of adsorbates on Au compared to Pd has important consequences for reactivity. In the absence of OH, methoxy reacts in the top site. Compared to the case on Pd(111), the transition-state energy is lower relative to the most stable adsorbed state of methoxy in part because of the reduced affinity for methoxy adsorption; the absence of purely Pd threefold hollow sites eliminates the favored sites. On the other hand, surface OH clearly does not enhance reactivity on PdAu(111), likely because OH is required to bind to the Au surface to be in close proximity for the methoxy on the model surface. Overall, the bimetallic surface has two clear effects: it

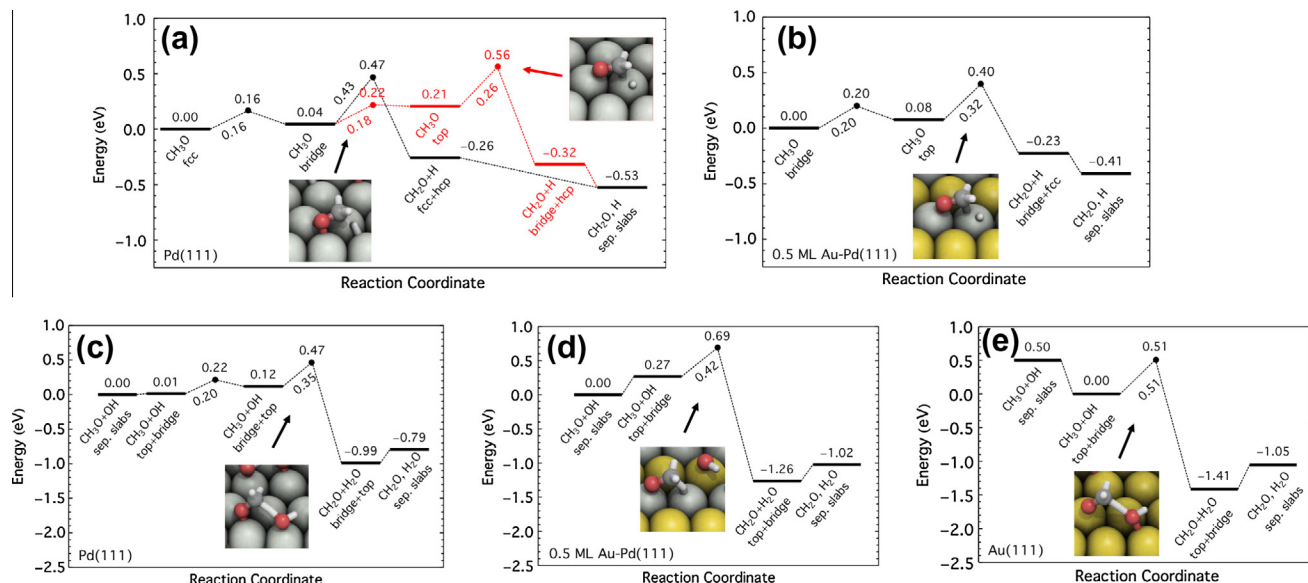


**Fig. 9.** Potential energy diagrams for methyl dehydrogenation (a and b) without OH and (c–e) with OH (note the change in scales between rows). The black path in panel (a) is the path for dehydrogenation from the bridge site, while the red path is for dehydrogenation from the top site. (For interpretation of the references to color in this figure legend, the reader is referred to the web version of this article.)

weakens adsorption relative to Pd(111) and generates ensembles of Pd atoms that restrict C–H scission steps to certain geometries.

## 4. Discussion

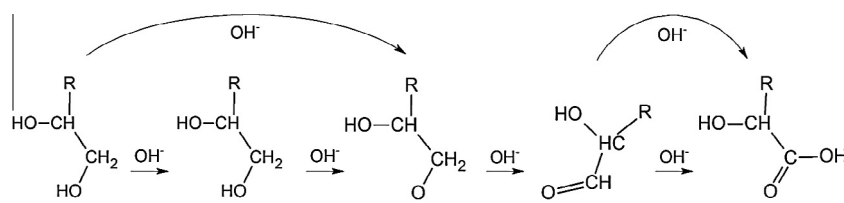
### 4.1. Mechanism

The results of this and other work have led to the development of a reaction mechanism for the oxidation of ethylene glycol and 1,2-propanediol on Pd/C, Au/C, and Au–Pd/C, shown in Scheme 2 [42,48]. Curved arrows represent reactions that can occur in the liquid phase without direct interaction with the catalyst. For the sake of clarity, only the major reaction pathway is included and all products are illustrated in their hydrogenated form. The first step is hydrogen abstraction from the primary hydroxyl group which can occur in solution or on the surface of the catalyst [48]. The resulting alkoxide undergoes C–H bond scission in the rate-determining step. In the presence of water, this is followed by the quick conversion of the aldehyde intermediate into the acid product, which proceeds through a transient geminal diol structure [2,4]. Although they are not shown in Scheme 2, small amounts of pyruvate and acetate were formed from further oxidation of lactate. These products only represent a small portion of the product distribution, and the pathways through which they are formed are not considered to be major contributors to the chemistry. Other reaction pathways involving tautomerization or Cannizzaro-type reactions cannot be ruled out. However, they are

not thought to be major contributors since there is no evidence of hydroxyacetone or pyruvaldehyde formation. Similarly, the high selectivity toward monoacids suggests that only one hydroxyl group is highly reactive in this system. Although oxygen is not directly involved in the mechanism, it is necessary in order to close the catalytic cycle and regenerate surface-bound hydroxide ions [48].

### 4.2. Selectivity

When ethylene glycol and 1,2-propanediol are studied on single crystals under vacuum conditions, both hydroxyl groups interact with the surface and are oxidized [18,50–55]. However, in the liquid phase, the surface is more crowded, and there is greater competition for active sites. Under these conditions, it becomes difficult for adsorbates to form more than one bond with the catalyst. For this reason, the conversion of a single hydroxyl group is favored, which explains the high selectivity toward glycolate and lactate seen in this work. High coverage could also explain the low reactivity of 1,2-propanediol's secondary hydroxyl group, which is more sterically hindered than the adjacent primary hydroxyl group and may not be able to interact with the surface. Conversion of the secondary hydroxyl group is also inhibited by an increased barrier to dehydrogenation, which has been established in ultra-high vacuum studies of alcohols and polyols on Pd surfaces [17,18].



**Scheme 2.** A proposed reaction mechanism for the oxidation of ethylene glycol and 1,2-propanediol on Pd/C, Au/C, and Au–Pd/C. Curved arrows represent reactions that can occur in the liquid phase without direct interaction with the catalyst. For the sake of clarity, only the major reaction pathway is included and all products are illustrated in their hydrogenated form.

In the case of 1,2-propanediol, the formation of lactate is accompanied by small amounts of pyruvate and acetate. The production of pyruvate was highest on the monometallic Pd catalyst, barely detectable on the bimetallic catalysts, and not observed on the monometallic Au catalyst. This trend is expected due to the inability of Au to oxidize the secondary hydroxyl group of 1,2-propanediol which ultimately leads to pyruvate production [10]. Acetate was produced on both of the monometallic catalysts but was hardly detectable on the bimetallic catalysts. It has been proposed that the decarbonylation of alcohols and polyols, which is necessary in order to form acetate, proceeds through a flat lying acyl intermediate [17,18]. It has also been shown that disrupting the periodicity of a catalytic surface through the addition of a modifying agent can inhibit an intermediate's ability to adopt a flat lying adsorption geometry [56]. It is possible that by forming a bimetallic surface, the structure is altered in such a way to inhibit decarbonylation, which would explain the decrease in acetate production on the bimetallic catalysts. This is in agreement with previous studies that show suppressed production of acetic acid from 1,2-propanediol on Pt catalysts doped with Pb, Bi, and Sn [57].

#### 4.3. Rate-limiting step

The primary kinetic isotope effect observed for  $d_4$ -ethylene glycol suggests that scission of the C–H bond determines the kinetics of ethylene glycol oxidation. In this case, it is likely that the presence of hydroxide ions leads to facile activation of the hydroxyl group and formation of an alkoxide surface intermediate. The lack of a primary kinetic isotope effect for the oxidation of  $d_2$ -ethylene glycol suggests that O–H bond activation does not influence the overall kinetics. This is in agreement with previous studies of alcohol oxidation which have shown a low barrier to O–H scission under alkaline conditions both in solution and on the surface of Au catalyst [48]. However, the possibility that hydrogen and deuterium may be exchanged between water and the hydroxyl groups cannot be eliminated, so it remains plausible that the O–H activation energy could affect the rate.

#### 4.4. Activity

Many different theories have been proposed to explain the superior activity of Au–Pd bimetallic catalysts for oxidation of alcohols. Some studies have suggested that the increased rates may be due to an alteration of the metal lattice [10,12]. If that were the case, significant increases in reaction rates would not be expected on catalysts prepared using electroless deposition, in which Au is deposited preferentially on the surface of Pd without affecting the underlying lattice structure [21,25]. Other explanations suggest that Au–Pd catalysts are less susceptible to oxygen poisoning, which leads to an increase in the availability of active sites and prolonged catalyst lifetime [10,11,16]. Severe oxygen poisoning during the course of a reaction results in a deviation from the initial rate constant as the catalyst is deactivated [58]. Such behavior is not obvious in this work. Previous studies have demonstrated that deactivation can occur before the reaction begins if the catalyst is exposed to oxygen prior to the reactant [59]. In this work, the reactant was injected before oxygen was introduced in order to avoid this situation. For these reasons, it is unlikely that the increased activity of the bimetallic catalyst is due exclusively to an enhanced resistance to oxygen poisoning. A third explanation suggests that changes in the electronic structure may be responsible for the increased activity of Au–Pd catalysts [10,12]. The experimental and computational results presented here support this hypothesis by showing a shift in the binding energy of Au core-level electrons as Au is added to Pd. A fourth explanation is that

**Table 7**

Activation energies for  $\text{CH}_3\text{O}$  dehydrogenation relative to the metastable state ( $E_{\text{act}}$ ) and to the initial state ( $E_{\text{trans}}$ ).

Surface	$E_{\text{act}}$	$E_{\text{trans}}$
Pd(111)	0.26	0.47
0.25Au–Pd(111)	0.32	0.40
Au(111)	0.51	0.51

ensemble effects may affect activity by changing adsorbate binding strength or geometry. This explanation is also supported by the DFT results. Electronic structure modifications and ensemble effects can affect activity by changing the intrinsic rate or changing the number of free sites available for reaction [60].

Although the DFT results are for a model system, they can provide significant insight into electronic structure modifications and ensemble effects. The d-band center of Pd experiences small shifts upon addition of Au, increasing by 0.01 eV for the 0.25 ML alloy and by 0.02 eV for the 0.5 ML alloy. Since all the adsorbates prefer to bind to Pd atoms over Au atoms, the electronic structure modifications are the only change when comparing Pd(111) and 0.25Au–Pd(111). An increase in the d-band center generally results in stronger adsorption, as seen for H, water, and methanol. However, the other adsorbates are destabilized upon adding Au. This trend has been previously seen for adsorbates with nearly full valence shells on alloys with nearly full d-bands and is due to electron–electron repulsion between the adsorbate and metal [61]. However, the small shifts observed for AuPd alloys would be expected to have a fairly small effect on adsorption energies, as is seen when comparing Pd(111) to 0.25Au–Pd(111). On 0.5Au–Pd(111), larger decreases in adsorption strength are seen for adsorbates that prefer the hollow site, as these adsorbates are forced to either bind to gold atoms or move to the bridge site. Hence, both electronic structure modifications and ensemble effects influence adsorption energies, with ensemble effects causing more dramatic variations when they occur. The ensemble effects also influence site preference.

Weaker methoxy adsorption leads to less favorable transfer of H to the surface, increasing the barriers for methoxy dehydrogenation from a given site. Hence, Pd(111) should have the highest intrinsic activity since the dehydrogenation barrier is the lowest (see the first column of Table 7). However, Sabatier analysis implies that on surfaces that bind adsorbates strongly, activation energies will be low but the surface will become too crowded to maintain a high rate [60]. This crowding effect could explain the low rate on Pd. Therefore, electronic structure modifications to Pd atoms as well as ensemble effects may increase activity on the alloys over pure Pd by weakening adsorption and freeing up surface sites.

For methoxy on 0.5Au–Pd(111), the hollow site is less favorable than the bridge site, resulting in one less diffusion step before dehydrogenation. Hence, even though dehydrogenation from the same site is less favorable on the bimetallic than on Pd, the transition state is lower relative to the initial state. Thus, the change in methoxy's site preference, which is due to ensemble effects, may increase its reactivity.

The lower rate on Au is likely due to the higher barrier for methoxy dehydrogenation. A further factor is that dehydrogenation on Au is a bimolecular process which may happen less frequently since it cannot occur in the absence of a nearby hydroxyl group. In summary, electronic effects and ensemble effects both weaken adsorption on the alloys as compared to pure Pd, which may increase activity by freeing up surface sites. Ensemble effects have more dramatic effects when they occur, and they may also cause alkoxides to adsorb in more reactive sites. The enhancement in activity of the alloys over Au is likely due to a decrease in the barrier for C–H scission.

## 5. Conclusions

The oxidation of ethylene glycol and 1,2-propanediol on Pd/C, Au/C, and Au–Pd/C catalysts produces glycolate (from ethylene glycol) and lactate (from 1,2-propanediol) with high selectivity. Significant rate enhancements are observed on each of the bimetallic catalysts. Investigations using selectively deuterated reagents reveal that C–H scission of ethylene glycol is the rate-determining step on Au/C and Au–Pd/C catalysts. DFT and XPS studies suggest that the rate enhancement on the bimetallic surfaces compared to Pd is likely due to a decrease in coverage of strongly bound adsorbates, while the enhancement over Au is likely due to a decrease in the barrier for C–H scission.

## Acknowledgments

The authors acknowledge support from the National Science Foundation (Awards CBET-0854251 and CBET-0854339) and the Colorado Center for Biorefining and Biofuels for funding this research. AAR acknowledges support from the Alfred P. Sloan Foundation. This work used the Extreme Science and Engineering Discovery Environment (XSEDE) under Grant Number TG-CHE040023N, which is supported by National Science Foundation Grant Number OCI-1053575. We also acknowledge supercomputing time at the Center for Nanoscale Materials at Argonne National Laboratory, supported by the U.S. Department of Energy, Office of Basic Energy Sciences, under Contract DE-AC02-06CH11357.

## References

- [1] C. Zhou, J.N. Beltramini, Y. Fan, G.Q. Lu, *Chem. Soc. Rev.* 37 (2008) 527.
- [2] T. Mallat, A. Baiker, *Chem. Rev.* 104 (2004) 3037.
- [3] B. Kattryniok, H. Kimura, E. Skrzyszowska, J. Girardon, P. Fongarland, M. Capron, R. Ducoulombier, N. Mimura, S. Paul, F. Dumeignil, *Green Chem.* 13 (2011) 1960.
- [4] M. Besson, P. Gallezot, *Catal. Today* 57 (2000) 127.
- [5] C.P. Vinod, K. Wilson, A.F. Lee, *J. Chem. Technol. Biotechnol.* 86 (2011) 161.
- [6] M.S. Lindblad, Y. Liu, A.C. Albertsson, E. Ranucci, S. Karlsson, *Adv. Polym. Sci.* 157 (2002) 139.
- [7] R. Datta, M. Henry, *J. Chem. Technol. Biotechnol.* 81 (2006) 1119.
- [8] T. Tsujino, S. Ohigashi, S. Sugiyama, K. Kawashiro, H. Hayashi, *J. Mol. Catal.* 71 (1992) 25.
- [9] T. Mallat, Z. Bodnar, C. Bronnimann, A. Baiker, *Platinum-Catalyzed Oxidation of Alcohols in Aqueous-Solutions – The Role of Bi-Promotion in Suppression of Catalytic Deactivation*, Elsevier Science Publ B V, Amsterdam, 1994, p. 385.
- [10] C. Bianchi, F. Porta, L. Prati, M. Rossi, *Top. Catal.* 13 (2000) 231.
- [11] M. Haruta, M. Date, *Appl. Catal. A* 222 (2001) 427.
- [12] H.J. Zhang, T. Watanabe, M. Okumura, M. Haruta, N. Toshima, *Nat. Mater.* 11 (2012) 49.
- [13] G.L. Brett, P.J. Miedziak, N. Dimitratos, J.A. Lopez-Sanchez, N.F. Dummer, R. Tiruvalam, C.J. Kiely, D.W. Knight, S.H. Taylor, D.J. Morgan, A.F. Carley, G.J. Hutchings, *Catal. Sci. Technol.* 2 (2012) 97.
- [14] D.I. Enache, J.K. Edwards, P. Landon, B. Solsona-Espriu, A.F. Carley, A.A. Herzing, M. Watanabe, C.J. Kiely, D.W. Knight, G.J. Hutchings, *Science* 311 (2006) 362.
- [15] M.S. Chen, D. Kumar, C.W. Yi, D.W. Goodman, *Science* 310 (2005) 291.
- [16] N. Dimitratos, A. Villa, D. Wang, F. Porta, D.S. Su, L. Prati, *J. Catal.* 244 (2006) 113.
- [17] J.L. Davis, M.A. Barteau, *Surf. Sci.* 187 (1987) 387.
- [18] M.B. Griffin, E.L. Jorgensen, J.W. Medlin, *Surf. Sci.* 604 (2010) 1558.
- [19] S. Carrettin, P. McMorn, P. Johnston, K. Griffin, C.J. Kiely, G.J. Hutchings, *Phys. Chem. Chem. Phys.* 5 (2003) 1329.
- [20] M. BeltowskaBrzezinska, T. Luczak, R. Holze, *J. Appl. Electrochem.* 27 (1997) 999.
- [21] J. Rebelli, A.A. Rodriguez, S. Ma, C.T. Williams, J.R. Monnier, *Catal. Today* 160 (2011) 170.
- [22] G.C. Bond, C. Lewis, D.T. Thompson, *Catalysis by Gold*, Imperial, London, 2006.
- [23] G. Kyriakou, M.B. Boucher, A.D. Jewell, E.A. Lewis, T.J. Lawton, A.E. Baber, H.L. Tierney, M. Flytzani-Stephanopoulos, E.C.H. Sykes, *Science* 335 (2012) 1209.
- [24] M.T. Schaal, M.P. Hyman, M. Rangan, S. Ma, C.T. Williams, J.R. Monnier, *J.W. Medlin, Surf. Sci.* 603 (2009) 690.
- [25] J. Rebelli, M. Detwiler, S. Ma, C.T. Williams, J.R. Monnier, *J. Catal.* 270 (2010) 224.
- [26] G. Kresse, J. Furthmüller, *Comp. Mater. Sci.* 6 (1996) 15.
- [27] G. Kresse, J. Hafner, *Phys. Rev. B* 47 (1993) 558.
- [28] J.P. Perdew, Y. Wang, *Phys. Rev. B* 45 (1992) 13244.
- [29] P.E. Blochl, *Phys. Rev. B* 50 (1994) 17953.
- [30] G. Kresse, D. Joubert, *Phys. Rev. B* 59 (1999) 1758.
- [31] J. Hafner, *J. Comp. Chem.* 29 (2008) 2044.
- [32] J.N. Andersen, D. Hennig, E. Lundgren, M. Methfessel, R. Nyholm, M. Scheffler, *Phys. Rev. B* 50 (1994) 17525.
- [33] S. Grimme, *J. Comp. Chem.* 27 (2006) 1787.
- [34] M. Amft, S. Lebegue, O. Eriksson, N.V. Skorodumova, *J. Phys.: Condens. Matter* 23 (2011) 1.
- [35] M. Tarini, P. Cignoni, C. Montani, *IEEE Trans. Vis. Comput. Gr.* 12 (2006) 1237.
- [36] S. Deki, K. Akamatsu, Y. Hatakenaka, M. Mizuhata, A. Kajinami, *Nanostruct. Mater.* 11 (1999) 59.
- [37] A.M. Venezia, L.F. Liotta, G. Pantaleo, V. La Parola, G. Deganello, A. Beck, Z. Koppány, K. Frey, D. Horvath, L. Guzzi, *Appl. Catal. A* 251 (2003) 359.
- [38] A.M. Venezia, V. La Parola, V. Nicoli, G. Deganello, *J. Catal.* 212 (2002) 56.
- [39] F. Liu, D. Wechsler, P. Zhang, *Chem. Phys. Lett.* 461 (2008) 254.
- [40] A. Ruban, B. Hammer, P. Stoltze, H.L. Skriver, J.K. Nørskov, *Mol. Cat. A: Chem.* 115 (1997) 421.
- [41] N. İnoğlu, J.R. Kitchin, *Mol. Simul.* 36 (2010) 633.
- [42] N. Dimitratos, J.A. Lopez-Sanchez, S. Meenakshisundaram, J.M. Anthonykutti, G. Brett, A.F. Carley, S.H. Taylor, D.W. Knight, G.J. Hutchings, *Green Chem.* 11 (2009) 1209.
- [43] F.H. Westheimer, *Chem. Rev.* 61 (1961) 265.
- [44] A. Schwartz, L.L. Holbrook, H. Wise, *J. Catal.* 21 (1971) 199.
- [45] W.J.C. Orr, *Trans. Faraday Soc.* 32 (1936) 1033.
- [46] H. Kwart, L.P. Kuhn, E.L. Bannister, *J. Am. Chem. Soc.* 76 (1954) 5998.
- [47] L. Kaplan, *J. Am. Chem. Soc.* 76 (1954) 4645.
- [48] B.N. Zope, D.D. Hibbitts, M. Neurock, R.J. Davis, *Science* 330 (2010) 74.
- [49] B. Xu, J. Haubrich, T.A. Baker, E. Kaxiras, C.M. Friend, *J. Phys. Chem. C* 115 (2011) 3703.
- [50] M. Bowker, R.J. Madix, *Surf. Sci.* 116 (1982) 549.
- [51] O. Skoplyak, M.A. Barteau, J.G. Chen, *Surf. Sci.* 602 (2008) 3578.
- [52] N.F. Brown, M.A. Barteau, *J. Phys. Chem.* 98 (1994) 12737.
- [53] R.J. Madix, T. Yamada, S.W. Johnson, *Appl. Surf. Sci.* 19 (1984) 43.
- [54] A.J. Capote, R.J. Madix, *J. Am. Chem. Soc.* 111 (1989) 3570.
- [55] C.R. Ayre, R.J. Madix, *Surf. Sci.* 303 (1994) 297.
- [56] M.B. Griffin, S.H. Pang, J.W. Medlin, *J. Phys. Chem. C* 116 (2012) 4201.
- [57] H. Pinxt, B.F.M. Kuster, G.B. Marin, *Appl. Catal. A* 191 (2000) 45.
- [58] P.J.M. Dijkgraaf, M.J.M. Rijk, J. Meuldijk, K. Vanderwiele, *J. Catal.* 112 (1988) 329.
- [59] P.J.M. Dijkgraaf, H.A.M. Duisters, B.F.M. Kuster, K. Vanderwiele, *J. Catal.* 112 (1988) 337.
- [60] T. Bligaard, J.K. Nørskov, S. Dahl, J. Matthiesen, C.H. Christensen, J. Sehested, *J. Catal.* 224 (2004) 206.
- [61] H. Xin, S. Linic, *J. Chem. Phys.* 132 (2010) 221101.